

The Kovacs memory effect in a thin granular layer: experimental evidence and its physical origin

Francisco Vega Reyes,^{1,*} Álvaro Rodríguez-Rivas,^{2,†} Pablo Maynar,^{3,‡} and M. Isabel García de Soria^{3,§}

¹*Departamento de Física and Instituto de Computación Científica Avanzada (ICCAEx),
Universidad de Extremadura, 06071 Badajoz, Spain*

²*Departamento de Matemática Aplicada II, Universidad de Sevilla,
E.T.S. de Ingeniería, C. de los Descubrimientos,
s/n. Pabellón Pza. de América 41092 Sevilla (Spain)*

³*Física Teórica, Universidad de Sevilla, Apartado de Correos 1065, 41080 Sevilla, Spain*

(Dated: February 25, 2026)

We report the experimental observation of memory effects in a vertically vibrated thin granular layer. Following a quench in the input acceleration, the granular temperature exhibits an anomalous Kovacs memory effect confined to the initial fast relaxation stage. This memory vanishes shortly thereafter, yielding a time-dependent memoryless regime governed solely by the instantaneous temperature before the system reaches its final steady state. We develop a kinetic theory framework that quantitatively captures these features by identifying the initial memory and subsequent memoryless regimes with the kinetic and hydrodynamic states, respectively (that are well established in kinetic theory). Our analysis reveals that memory emerges during fast transients through coupling between horizontal and vertical temperatures—a mechanism that fundamentally constrains the accessible memory phenomenology and precludes observation of the standard Kovacs effect in this system. Molecular dynamics simulations provide independent confirmation of all experimental and theoretical findings.

Introduction—In physical systems, *memory* refers to the ability to encode information about past states in a manner that influences subsequent evolution [1]. The study of memory formation has attracted growing interest due to its broad relevance across nonequilibrium physics. Within this context, two phenomena have been studied extensively: the Mpemba and Kovacs effects. The Mpemba effect describes anomalous relaxation whereby a hotter (or colder) system may reach thermal equilibrium faster than a cooler (or hotter) one [2, 3]. The Kovacs effect, initially observed in polymers [4] and later extended to active and granular matter [5–9], manifests as a system’s tendency to transiently revert toward a past state during relaxation toward a stationary state.

Granular fluids provide a compelling platform for exploring such memory effects. Previous experimental work has examined memory in the compaction of shaken granular layers [10] and the Mpemba and Kovacs effects have been theoretically studied in driven granular gases [2, 11]. The Kovacs effect appears as non-monotonic evolution of an observable—typically volume, stress, or temperature—upon resuming relaxation after an intermediate perturbation. Notably, far-from-equilibrium analyses predict an *anomalous* Kovacs response in which relaxation initially proceeds in the same direction as before the perturbation, driving the system further from its instantaneous target state [6, 11]; see Fig. 1.

Despite these theoretical developments, experimental evidence of memory effects in granular fluids remains scarce, though the Mpemba effect has been reported in other systems [12]. In this Letter, we present the first ex-

perimental observation of the Kovacs effect in granular matter. In particular, we reveal a robust memory signature associated with the granular temperature (i.e., the average particle kinetic energy) [13]. In contrast to earlier studies focused on density [10] or stress [14], our results demonstrate memory effects directly through thermal relaxation dynamics.

Since particle collisions are inelastic, a steady state in granular matter can only be achieved through sustained energy input, the intensity of which is here described by the parameter Γ [15–18]. The thermal Kovacs cooling protocol proceeds as follows [4, 6, 8]: a granular fluid initially at stationary temperature T_0 (the energy input being Γ_0) is quenched (by lowering the energy input to Γ_s) at time t_0 and relaxes monotonically toward a new stationary state $T_s < T_0$, that would be reached at a long time t_s . However, at an intermediate waiting time t_w (where $t_0 < t_w < t_s$), the energy injection is adjusted to $\Gamma_w > \Gamma_s$ so that the new stationary temperature T_s^* equals the instantaneous temperature: $T(t_w) = T_s^* > T_s$ [11, 19]. In a *normal* Kovacs response, dT/dt reverses sign at t_w , producing an upward hump. In an *anomalous* response, the sign is preserved and the system continues cooling, generating a downward hump (Fig. 1) [6, 8].

The Kovacs effect may appear paradoxical since it can occur even when all hydrodynamic variables equal their stationary values [4]. Memory is reflected in a non-monotonic behavior of the temperature, implying that, at those times, the temperature does not fully specify the state of the system. Kinetic theory explains this behavior through the distinction between *kinetic* and *hydrodynamic* regimes [13, 20–23]. The dynamics of the veloc-

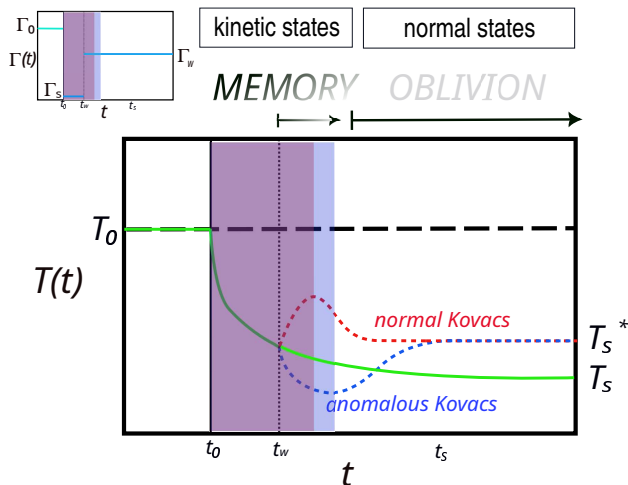


FIG. 1. Schematic representation of the Kovacs cooling protocol and the two kinds of memory effects considered. The granular fluid initially at stationary temperature T_0 (the energy input being Γ_0) is quenched by lowering the energy input to Γ_s at time t_0 and relaxes monotonically toward a new stationary state $T_s < T_0$, that would be reached at a long time t_s (green solid line). However, at an intermediate waiting time t_w (where $t_0 < t_w < t_s$), the energy injection is adjusted to Γ_w so that the new stationary temperature T_s^* equals the instantaneous temperature: $T(t_w) = T_s^* > T_s$. The normal Kovacs effect is produced in the form of an upwards hump of the temperature, and hence $\text{sg}(dT/dt|_{t_w^-}) \neq \text{sg}(dT/dt|_{t_w^+})$. In this case, the system temporarily tends to reach the initial state that the system had at $t = t_0$ (red dot line). On the contrary, the anomalous Kovacs effect is characterized by a downwards hump and now $\text{sg}(dT/dt|_{t_w^-}) = \text{sg}(dT/dt|_{t_w^+})$ where the system tries to continue cooling down (blue dot line), as if it remembered the previous relaxation process instead. In both cases, the system remembers features of the past. The top left inset shows the corresponding changes of the input signal Γ .

ity distribution function consists of a rapid and initial-condition-dependent evolution (the kinetic regime) over a characteristic time t_m , followed by a hydrodynamic regime in which all the time dependence enters solely through the hydrodynamic fields, the granular temperature in our case. During the kinetic stage ($t \lesssim t_m$), the velocity distribution function depends on both T and higher-order moments $\{a, b, \dots\}$:

$$f(\mathbf{v}, t) = f(\mathbf{v} | T(t), a(t), b(t), \dots), \quad (1)$$

while in the hydrodynamic regime ($t \gtrsim t_m$), the distribution simplifies to

$$f(\mathbf{v}, t) = f(\mathbf{v} | T(t)), \quad (2)$$

and memory vanishes: the system cannot return to kinetic states unless perturbed anew [20, 23]. Clearly, the hydrodynamic fields specify the state of the system only in the hydrodynamic regime. In the kinetic regime, even when $T = T_s$, evolution of the moments $\{a, b, \dots\}$ can

drive further changes in T . In the Kovacs protocol described above, the system is typically in the hydrodynamic regime just before the quench and it is automatically driven out of it after the quench and memory effects may arise.

In this letter, we consider a thin vertically vibrated granular layer in which the walls move sinusoidally with amplitude, A , and angular frequency, ω . The energy input is thus measured by the mean dimensionless acceleration of the walls, $\Gamma \equiv A\omega^2/g$, with g being the gravitational acceleration. The base state of the fluid phase in this kind of system is homogeneous and the dynamics is quasi-2D [24]. Thus, the relevant hydrodynamic field is the horizontal granular temperature, $T = (m/2)\langle v_x^2 + v_y^2 \rangle$ [24, 25] (where $\langle \dots \rangle$ denotes particle average, m is particle mass and \mathbf{v} is particle velocity). By combining theory, simulations, and experiments, we demonstrate that (i) the Kovacs effect in vibrated thin granular layers is intrinsically anomalous, (ii) memory is confined to kinetic stages, and (iii) subsequent relaxation proceeds through a universal memoryless hydrodynamic state governed solely by the horizontal temperature. In addition, the results show that memory characteristics are constrained by the system's governing equations and cannot be tuned through external conditions alone.

Experimental configuration- Our experimental setup follows the design used in previous works by Urbach and co-workers [24, 26]; see Fig. 2. It consists of a thin, circular layer of N identical stainless-steel spheres (AISI 52100), with coefficient of normal restitution $\alpha = 0.95$ [27]. The spheres diameter is $\sigma \simeq 2.38$ mm. The layer is confined between a bottom aluminum plate and a top plexiglas lid, with steel spacers forming the lateral boundary. The separation between the plates, h , satisfies $\sigma < h < 2\sigma$, ensuring that particles cannot overlap while still allowing collisions with both vertical and horizontal components of the relative velocity. This geometry promotes efficient energy redistribution when the system is vertically vibrated by an electromagnetic shaker (the input signal has a form $A \sin(\omega t)$) and allows for horizontal particle position and velocity measurement [25, 28].

All experiments were performed at a driving frequency $\nu \equiv \frac{\omega}{2\pi} = 180$ Hz. The layer height was set to $h = 1.75\sigma$. The two-dimensional density was fixed at $\rho_{2D} = 0.45$, which corresponds to $N = 4711$ particles. Here, ρ_{2D} is defined following $\rho_{2D} \equiv N/N_{\max}$ [24, 29] with $N_{\max} = 10469$ being the maximum number of particles fitting into the circular domain under close packing. For additional details, including a list of the equipment used, see the Appendix A.

Molecular dynamics simulations- We performed molecular dynamics simulations, following an algorithm analogous to the one we used in previous works [24, 29]. Wall-particle and particle-particle collisions are inelastic and we model them by using a viscoelastic collisional model [24]. The walls move sinusoidally as in the experiment.

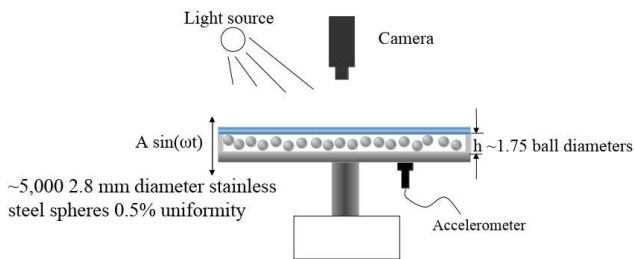


FIG. 2. Schematic representation of the experimental setup. The thin granular layer of steel spheres is vertically vibrated. The input acceleration $\Gamma = A\omega^2/g$ is monitored with an accelerometer, where A is the vibration amplitude, ω the angular frequency, and $g = 9.8 \text{ m/s}^2$.

Frequency and vibration amplitude may be controlled independently, as well as other relevant parameters in the system. For more details, see Appendix B.

Results— Through extensive experimental measurements and molecular dynamics simulations, we verify that our system exhibits exclusively the *anomalous* Kovacs effect (Figure 3). Following the protocol described above, after each quench at different waiting times t_w , the system will ultimately evolve towards stationary temperatures, T_s^* , that depend on Γ_w . However, prior to this, we observed in all cases that at t_w an extended cooling takes place during a finite time interval until reaching a minimum temperature T_{\min} at t_{\min} . Beyond this point, the temperature increases monotonically, ultimately reaching the steady value, T_s^* , as observed in all relaxation curves in Figure 3. To quantify the memory response amplitude, we define the anomalous Kovacs measure as $\mathcal{H}_{\min} = T_{\min}/T_s^* - 1$. Thus, $\mathcal{H}_{\min} < 0$ in our system. In Figure 3(a) for experiments and Figure 3(b) for simulations we can see that the memory amplitude \mathcal{H}_{\min} tends to decrease as $t_w \rightarrow t_s$, and it is expected to become null for $t_w = t_s$ since in that case the kinetic states have disappeared by definition (because the system is already in steady state). A more quantitative analysis of the behavior of the memory amplitude is performed in the *Theory* section.

We identify the onset of hydrodynamic behavior through a rigorous criterion: the point at which the next higher moment (kurtosis $K = \langle (v_x^2 + v_y^2)^2 \rangle / \langle (v_x^2 + v_y^2) \rangle^2$) becomes stationary. This is significant because once K reaches a constant value, all remaining time-dependence in the distribution function must occur exclusively through the lower-order moments—specifically, through the hydrodynamic field T . The system thus becomes effectively hydrodynamic. To verify this picture, we measured the kurtosis K relaxation (see Figure 1 in the Supplementary Material file for more detail) across all experimental and simulation series. We indicate, by means of vertical arrows in Figure 3, the times at which K becomes stationary (indicated by the arrows). Remarkably,

in all cases, the temperature minimum T_{\min} occurs before this hydrodynamic transition point. This temporal ordering directly demonstrates that the Kovacs memory effect—signaled by the non-monotonic temperature evolution—vanishes precisely when hydrodynamic behavior is established. Therefore, anomalous memory effects cannot persist in truly hydrodynamic states.

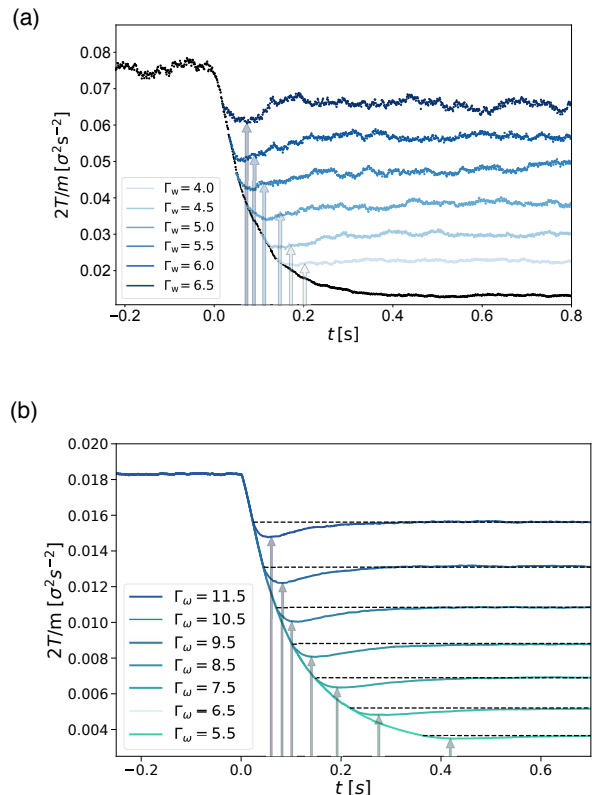


FIG. 3. Horizontal temperature (blue) relaxation curves for a Kovacs protocol in experiments and molecular dynamics simulations. (a) Experiments: $\nu = 180 \text{ Hz}$; initial and final acceleration inputs are $\Gamma_0 = 7.0$ and $\Gamma_f = 3.15$ respectively, while intermediate values of the input acceleration at different waiting times t_w are $\Gamma_w = \{6.5; 6.0; 5.5; 5.0; 4.5; 4.0\}$. (b) Molecular dynamics: $\nu = 643.22 \text{ Hz}$. $\Gamma_0 = 12.5$ and $\Gamma_f = 5.0$ respectively, and $\Gamma_w = \{11.5; 10.5; 9.5; 8.5; 7.5; 6.5; 5.5\}$. For both experiment and simulation, darker blue in the curves corresponds to higher Γ_w . Arrows mark the t_m values extracted from the time evolution of the kurtosis.

The transition to memoryless hydrodynamic behavior—which we have identified through the constancy of kurtosis—can also be demonstrated directly from the relaxation dynamics of the horizontal temperature. We analyze this in Figure 4, where the system initially at steady states with different Γ_0 , T_0 , converges to the same stationary temperature (due to a quench to the same value Γ_s). Thus, beyond the hydrodynamic threshold identified in the previous figure, Figure 4(a) shows experimentally that, after a convenient translation in the time axes, t_{Γ} , the horizontal temperature curves collapse onto

a single curve (in the previous initial transient, the system still remains in the aforementioned kinetic stage). This data collapse demonstrates that T is the unique hydrodynamic variable controlling long-time dynamics.

The simulations provide additional quantitative insight through access to the vertical temperature $T_z = m\langle v_z^2 \rangle$. Figure 4(b) plots T_z versus T for different initial conditions under both heating and cooling protocols. After an initial transient, T_z establishes a universal relationship with T , following a single curve toward a unique stationary state (marked with a cross). This collapse onto a universal manifold elegantly demonstrates how non-hydrodynamic modes relax onto the lower-dimensional manifold defined by the hydrodynamic variable T —directly confirming that once higher moments become stationary, all remaining evolution is governed by T alone.

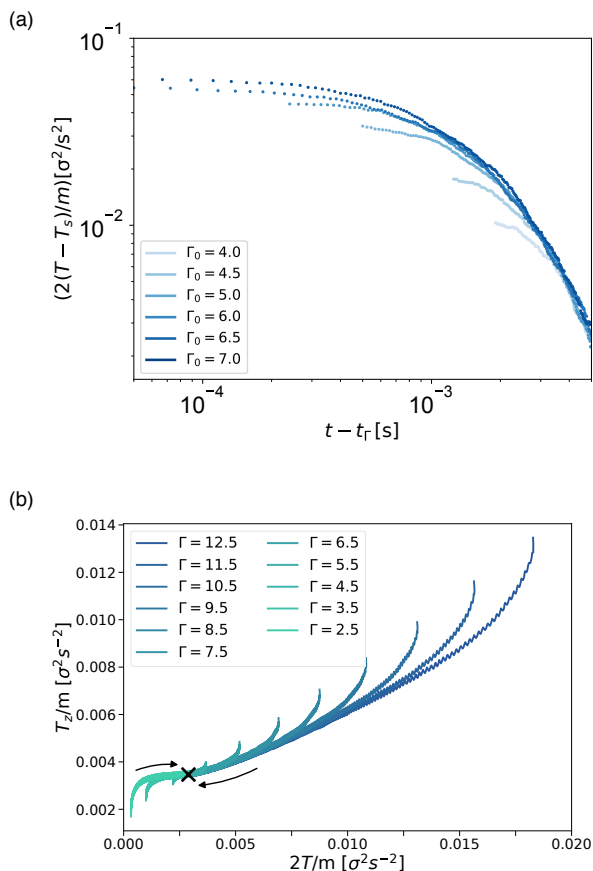


FIG. 4. (a) Relaxation curves T vs. t from experiments, for a step-down protocol with $\Gamma_s = 3.15$, and $\Gamma_0 = \{6.5; 6.0; 5.5; 5.0; 4.5; 4.0\}$. Here t_Γ denotes the translation in the time performed to each curve to make the curves collapse. (b) Relaxation curves of T_z vs. T from simulation data, for a series of values of initial input accelerations $\Gamma_0 = \{2.5; 3.5; 4.5; 5.5; 6.5; 7.5; 8.5; 9.5; 10.5; 11.5; 12.5\}$ to a final state with $\Gamma_s = 5.0$.

Theory- To explain the above phenomenology, we consider the simple microscopic model introduced in [30]:

an ensemble of N hard spheres of diameter σ that collide inelastically with a velocity independent coefficient of normal restitution, α , confined between two walls of area S separated a distance $h < 2\sigma$. The top wall is elastic, while the bottom wall mimics a vibrating sawtooth wall of mean velocity v_0 that injects energy into the system (details are given in the Supplementary Material (SM)). For this model, a kinetic equation can be formulated, i.e., a closed equation for the one-particle distribution function, $f(\mathbf{r}, \mathbf{v}, t)$, that accurately describes the dynamics of the system. For spatially homogeneous states, the horizontal and vertical temperatures, T and T_z , are defined as

$$nT = \int d\mathbf{v} \frac{m}{2} (v_x^2 + v_y^2) f(\mathbf{v}, t), \quad (3)$$

$$\frac{n}{2} T_z = \int d\mathbf{v} \frac{m}{2} v_z^2 f(\mathbf{v}, t), \quad (4)$$

where $n = \frac{N}{S(h-\sigma)}$ is the particle density. From the kinetic equation, assuming that the distribution function is a gaussian with different horizontal and vertical temperatures (in agreement with the results of the previous section), closed evolution for the temperatures are obtained to leading order in $\epsilon = (h - \sigma)/\sigma$, obtaining

$$\begin{aligned} \frac{dT}{dt} &= \sqrt{\frac{\pi T}{m}} (1 + \alpha) \epsilon n \sigma^2 \quad (5) \\ &\times \left[-(1 - \alpha)T + \epsilon^2 \left(-\frac{5\alpha - 1}{12} T + \frac{3\alpha + 1}{12} T_z \right) \right], \\ \frac{dT_z}{dt} &= \frac{2}{3} \sqrt{\frac{\pi T}{m}} (1 + \alpha) \epsilon^3 n \sigma^2 \left(\frac{1 + \alpha}{2} T - T_z \right) + \frac{2v_0}{\epsilon \sigma} T_z. \quad (6) \end{aligned}$$

The structure of the equations is clear: energy is injected in the vertical direction (last term of Eq. (6)), while it is transferred to the other degrees of freedom via inelastic collisions. In the long time limit, a stationary state is reached in which the energy injected by the bottom wall is compensated by the energy lost in collisions. As the energy is injected in the vertical direction, if the velocity of the bottom wall is suddenly changed at $t = t_w$, $dT/dt|_{t_w^-} = dT/dt|_{t_w^+}$, because v_0 does not explicitly appear in Eq. (5). Hence, for this model, only the anomalous Kovacs effect appears. Moreover, an analysis of Eqs. (5) and (6) indicates that, after a transient, the system forgets the initial condition and reaches a time-dependent solution in which the vertical temperature is slaved to the horizontal temperature [30]. This is exactly the same behavior that the one of the Molecular Dynamics simulations of the realistic model (see Fig. 4(b)). The stationary state is reached through this time-dependent universal solution indicating that the horizontal temperature is the relevant hydrodynamic variable in agreement to what happens in the experiments (see Fig. 4(a)). A

similar behavior appears in other heated granular models [31].

Close to the stationary state a more quantitative analysis can be done by linearizing Eqs. (5) and (6) around the stationary state (see SM). To study the shape of the hump, we introduce the function $\mathcal{H}(s) = T(s)/T_s - 1$, where s is proportional to the collisions per particle in (t_w, t) , $ds = (1 + \alpha) n \sigma^2 \epsilon \sqrt{\frac{\pi T_s}{m}} dt$. In the linear theory, the function $\mathcal{H}(s)$ can be explicitly calculated, obtaining

$$\mathcal{H}(s) = \frac{e^{\lambda_1 s} - e^{\lambda_2 s}}{\lambda_1 - \lambda_2} \left. \frac{d\mathcal{H}}{ds} \right|_{s=0}. \quad (7)$$

λ_1 and λ_2 are two dimensionless negative functions of α and ϵ (their explicit expressions are given in the SM) associated to two time scales: a fast scale associated to λ_2 and a slow scale (hydrodynamic scale) associated to λ_1 (actually, $\lim_{\alpha \rightarrow 1} \lambda_1 = 0$). As $\lambda_2 < \lambda_1 < 0$, $\text{sg}[\mathcal{H}(s)] = \text{sg}[\left. \frac{d\mathcal{H}}{ds} \right|_{s=0}]$. Since the cooling Kovacs protocol requires $\left. \frac{d\mathcal{H}}{ds} \right|_{s=0} < 0$, it follows that $\mathcal{H}(s) < 0$ (see Figure 3). Moreover, from Eq. (7), it follows that the time interval to reach the minimum (in the s -scale) measured from t_w does not depend on t_w and that the amplitude of the hump, \mathcal{H}_{\min} , is proportional to $\left. \frac{d\mathcal{H}}{ds} \right|_{s=0}$. This is in agreement with the results of Fig. 3, where it is shown that the amplitude of the hump decreases with the input acceleration.

Conclusions—We have provided unequivocal experimental evidence of Kovacs-type memory effects in a vertically vibrated confined granular gas. Remarkably, only the *anomalous* Kovacs response is observed: during relaxation, the system initially departs further from its target state, with complete absence of the classical (normal) Kovacs hump. This demonstrates that vertical energy injection combined with quasi-two-dimensional confinement fundamentally suppresses the normal memory response. Through a minimal kinetic theory model and molecular dynamics simulations, we establish that the dynamics is governed by two coupled temperatures—horizontal and vertical—operating on slow and fast timescales, respectively. The directional nature of energy injection directly constrains the accessible memory phenomenology, permitting only the anomalous Kovacs effect.

Our experiments reveal that memory effects are confined to the initial rapid transients (kinetic states)—a fundamentally different regime from persistent path-dependent memory in externally-driven systems (such as magnetic hysteresis), which encode the protocol history into structural degrees of freedom. Specifically, memory arises during the fast initial transient where both temperature components play a crucial role, while subsequent evolution follows a universal hydrodynamic state with constant kurtosis governed solely by the horizontal temperature.

This confinement of memory to kinetic regimes reveals

a universal principle grounded in projection operator formalism: memory emerges whenever a reduced or projected description fails—whether from persistence of kinetic moments (as here) or from slow-decaying Liouvillian modes (as in quantum control [32]). This insight is grounded in projection operator formalism: Zwanzig-Mori theory shows that eliminating degrees of freedom necessarily generates memory kernels [33–35]. These findings suggest that rational control of memory in driven dissipative systems requires explicit consideration of the underlying kinetic degrees of freedom and their relaxation timescales.

We thank Prof. A. Santos for useful comments on the early versions of this work and Profs. J. J. Brey and J. S. Urbach for later insightful discussion. We acknowledge support from Ministerio de Ciencia, Innovación y Universidades through Agencia Estatal de Investigación (AEI) through projects no. PID2020-116567GB-C22 (FVR), no. PID2024-156257NB-C21 (AR-R) and no. No. PID2021-126348NB-I00 (MIGS and PM) funded by MCIN/AEI/10.13039/501100011033 and ERDF “A way of making Europe”. F.V.R. also acknowledges support from Junta de Extremadura through contract No. GR24077 and MIGS and PM from the Grant No. ProyExcel-00505, funded by the Junta de Andalucía. The authors gratefully acknowledge the Centro Informático Científico de Andalucía (CICA), part of the Agencia Digital de Andalucía (ADA), for providing high-performance computing (HPC) resources from the Hércules Cluster and technical support.

* fvega@eaphysics.xyz

† arodriguezrivras@us.es

‡ maynar@us.es

§ gsoria@us.es

- [1] N. C. Keim, J. D. Paulsen, Z. Zeravcic, S. Sastry, and S. R. Nagel, Memory formation in matter, *Reviews of Modern Physics* **91**, 10.1103/revmodphys.91.035002 (2019).
- [2] A. Lasanta, F. Vega Reyes, A. Prados, and A. Santos, When the hotter cools more quickly: Mpemba effect in granular fluids, *Physical Review Letters* **119**, 10.1103/physrevlett.119.148001 (2017).
- [3] Z. Lu and O. Raz, Nonequilibrium thermodynamics of the markovian mpemba effect and its inverse, *Proceedings of the National Academy of Sciences* **114**, 5083–5088 (2017).
- [4] A. J. Kovacs, J. J. Aklonis, J. M. Hutchinson, and A. R. Ramos, Isobaric volume and enthalpy recovery of glasses. ii. a transparent multiparameter theory, *Journal of Polymer Science: Polymer Physics Edition* **17**, 1097–1162 (1979).
- [5] R. Kürsten, V. Sushkov, and T. Ihle, Giant kovacs-like memory effect for active particles, *Physical Review Letters* **119**, 10.1103/physrevlett.119.188001 (2017).
- [6] A. Prados and E. Trizac, Kovacs-like memory effect

- in driven granular gases, *Physical Review Letters* **112**, 10.1103/physrevlett.112.198001 (2014).
- [7] E. Trizac and A. Prados, Memory effect in uniformly heated granular gases, *Physical Review E* **90**, 012204 (2014).
- [8] J. J. Brey, M. I. García de Soria, P. Maynar, and V. Buzón, Memory effects in the relaxation of a confined granular gas, *Physical Review E* **90**, 032207 (2014).
- [9] A. Santos, Time-delayed newton's law of cooling with a finite-rate thermal quench: Impact on the mpemba and kovacs effects, *Physical Review E* **111**, 10.1103/physreve.111.055402 (2025).
- [10] C. Josserand, A. V. Tkachenko, D. M. Mueth, and H. M. Jaeger, Memory effects in granular materials, *Physical Review Letters* **85**, 3632–3635 (2000).
- [11] A. Lasanta, F. Vega Reyes, A. Prados, and A. Santos, On the emergence of large and complex memory effects in nonequilibrium fluids, *New Journal of Physics* **21**, 033042 (2019).
- [12] G. Teza, J. Bechhoefer, A. Lasanta, O. Raz, and M. Vucelja, Speedups in nonequilibrium thermal relaxation: Mpemba and related effects, *Physics Reports* **1164**, 1 (2026).
- [13] J. J. Brey, J. W. Dufty, C. S. Kim, and A. Santos, Hydrodynamics for granular flow at low density, *Physical Review E* **58**, 4638–4653 (1998).
- [14] D. Candela, Complex memory formation in frictional granular media, *Physical Review Letters* **130**, 10.1103/physrevlett.130.268202 (2023).
- [15] D. R. M. Williams and MacKintosh, Driven granular media in one dimension: Correlations and equation of state, *Physical Review E* **54**, R9 (1996).
- [16] A. Puglisi, V. Loreto, U. Marini Bettolo Marconi, A. Petri, and A. Vulpiani, Clustering and non-gaussian behavior in granular matter, *Physical Review Letters* **81**, 3848 (1998).
- [17] R. Caferio, S. Luding, and H. J. Herrmann, Two-dimensional granular gas of inelastic spheres with multiplicative driving, *Physical Review Letters* **84**, 6014 (2000).
- [18] R. Brito, D. Risso, and R. Soto, Hydrodynamic modes in a confined granular fluid, *Physical Review E* **87**, 022209 (2013).
- [19] E. Mompó, M. A. López-Castaño, A. Lasanta, F. Vega Reyes, and A. Torrente, Memory effects in a gas of viscoelastic particles, *Physics of Fluids* **33**, 10.1063/5.0050804 (2021).
- [20] D. Hilbert, Begründung der kinetischen Gastheorie, *Math. Ann.* **72**, 562 (1912).
- [21] C. Cercignani, *Mathematical methods in kinetic theory* (Springer Science + Business Media, New York, NY, USA, 1972).
- [22] S. Chapman and S. Cowling, *The mathematical theory of nonuniform gases* (Cambridge University Press, Cambridge, UK, 1970).
- [23] S. G. Brush, *Kinetic theory*, International Series of Monographs in Natural Philosophy 42, Vol. 3 (Pergamon Press, Oxford, UK, 1972).
- [24] P. Melby, F. Vega Reyes, A. Prevost, R. Robertson, P. Kumar, D. A. Egolf, and J. S. Urbach, The dynamics of thin vibrated granular layers, *Journal of Physics: Condensed Matter* **17**, S2689–S2704 (2005).
- [25] J. S. Olafsen and J. S. Urbach, Clustering, order, and collapse in a driven granular monolayer, *Phys. Rev. Lett.* **81**, 4369 (1998).
- [26] J. S. Olafsen and J. S. Urbach, Velocity distributions and density fluctuations in a granular gas, *Physical Review E* **60**, R2468–R2471 (1999).
- [27] M. Louge and et al., Fall 1999 impact parameter chart (1999).
- [28] J. C. Crocker and D. G. Grier, Methods of digital video microscopy for colloidal studies, *Journal of Colloid and Interface Science* **179**, 298–310 (1996).
- [29] F. Vega Reyes and J. S. Urbach, Effect of inelasticity on the phase transitions of a thin vibrated granular layer, *Physical Review E* **78**, 10.1103/physreve.78.051301 (2008).
- [30] P. Maynar, M. I. García de Soria, and J. Javier Brey, Homogeneous dynamics in a vibrated granular monolayer, *Journal of Statistical Mechanics: Theory and Experiment* **2019**, 093205 (2019).
- [31] M. I. García de Soria, P. Maynar, and E. E. Trizac, Universal reference state in a driven homogeneous granular gas, *Physical Review E* **85**, 051301 (2012).
- [32] N. Beato and G. Teza, Relaxation control of open quantum systems, *Phys. Rev. Lett.* **136**, 070401 (2026).
- [33] R. W. Zwanzig, Ensemble method in the theory of irreversibility, *The Journal of Chemical Physics* **33**, 1338 (1960).
- [34] H. Mori, A continued-fraction representation of the time-correlation functions, *Progress of Theoretical Physics* **34**, 399 (1965).
- [35] D. Forster, *Hydrodynamic Fluctuations, Broken Symmetry, and Correlation Functions* (W. A. Benjamin, 1975).
- [36] D. B. Allan, T. Caswell, N. C. Keim, C. M. van der Wel, and R. W. Verweij, soft-matter/trackpy: v0.7 (2025).
- [37] X. Nie, E. Ben-Naim, and S. Y. Chen, Dynamics of vibrated granular monolayers, *Europhysics Letters (EPL)* **51**, 679–684 (2000).
- [38] J. Sun, F. Battaglia, and S. Subramaniam, Dynamics and structures of segregation in a dense, vibrating granular bed, *Physical Review E* **74**, 10.1103/physreve.74.061307 (2006).

Appendix A: Experimental Methods

The experiments were performed using a Brüel & Kjær vibration system composed of an amplifier (LDS LPA600), controller (Comet COM200), and electromagnetic shaker (LDS V406) with an internal amplifier (PA500L). The system delivers up to 196 N of force and a maximum peak-to-peak displacement of 17.6 mm. A triaxial accelerometer (model 4535-B, sensitivity 10 mV/g, range 700 g) provides precise closed-loop control of the vertical acceleration. It measures also the horizontal acceleration, which helps to achieve very accurate horizontality of the thin layer. We checked that input acceleration fluctuations remain below 1%. System operation and monitoring are performed using Brüel & Kjær software (SCO-02V). The shaker is cooled by a 50 Hz fan to ensure stable performance, and a low-frequency absorption plug is mounted beneath the plate to suppress low-frequency noise in the accelerometer input signal.

A Phantom VEO high-speed camera records the particle motion at 1000 fps. Camera triggering and acceleration changes are synchronized using a Keysight DSOX2024A oscilloscope (4 channels, 200 MHz bandwidth, ~ 1 GS/s sampling rate). This arrangement allows frame-level precision in identifying the instant of acceleration change, which is essential for protocol timing.

The granular material consists of stainless steel spheres (AISI 52100) disposed over a circular plate of anodized aluminum. The particle-particle with coefficient of restitution is $\alpha = 0.95$ [27]. The gap spacing (system height) is $h = 1.75\sigma$ is obtained with the use of stainless steel ring-shaped spacers so that their inner diameter is $L = 256$ mm. The driving frequency is $\nu = 180$ Hz. A photograph of the setup is shown in Fig. A1. The spheres have a diameter $\sigma = 3/32$ in $\simeq 2.38252$ mm ± 0.5 μ m, mass density $\rho = 7833.4$ kg/m³, and mass $m = 0.0555$ g. The 2D particle density in the experiments is $\rho_{2D} = 0.45$. The density definition follows previous studies [24, 29]: $\rho_{2D} \equiv N/N_{\max}$, where $N_{\max} = 10469$ is the maximum number of balls used in the experiments that can fit in a hexagonally arranged 2D lattice in the circular plate of our set-up; i.e., $N_{\max}\sigma^2/L^2 \equiv \pi/(2\sqrt{3})$ and thus, in the experiments, we use $N = 4711$ particles.

Movies of the experiments are recorded through the transparent lid. With suitable lighting, particle horizontal positions are extracted and tracked with high accuracy [25], so that the 2D horizontal dynamics can be analyzed. We use the Crocker–Grier algorithm [28], in the Python implementation of Allan *et al.* [36], modified to suit our needs.

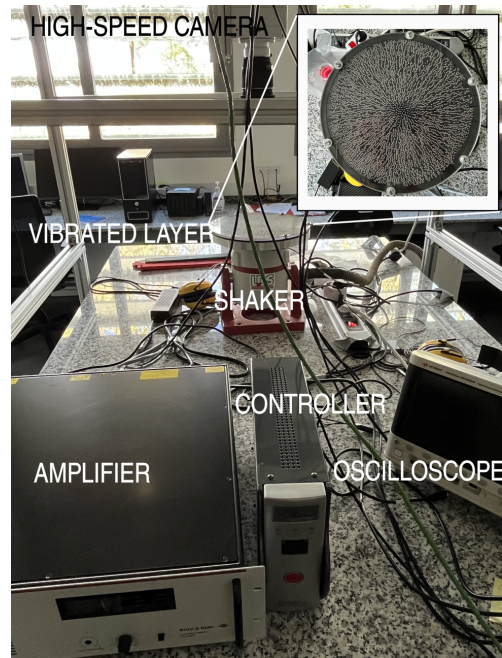


FIG. A1. Experimental setup in our laboratory (Instituto de Computación Científica Avanzada, ICCAEx, Badajoz, Spain). Inset: top-view close-up of the granular layer.

Protocol preparation.— The protocol follows Appendix A. Steps 1 and 2 simply require driving the system at the desired acceleration, maintained by the closed-loop controller. In step 3, the layer is driven at $\Gamma = 7.0$ and then switched to $\Gamma = 3.5$ after a sufficiently long time. The entire process is recorded, enabling extraction of the horizontal granular temperature. The control signals from the vibration system and camera are fed to the oscilloscope, allowing identification of the frame in which the acceleration change occurs. The camera resolution is 1 ms (1000 fps), and the vibration refresh time during this step is $1/f = 5.5$ ms, allowing accurate synchronization.

The intermediate steady temperatures $\{T_s^i\}$ from step 2 are used to identify the frames in step-3 at which the corresponding temperatures are reached, which is needed for steps 4–5. Experimentally, these steps proceed by preparing the system in the steady state at $\Gamma = 7.0$, switching to $\Gamma = 3.15$, waiting the required number of cycles, and then switching to the appropriate intermediate Γ^i . Reference times for all switches are obtained from the oscilloscope traces, as in step 3.

Appendix B. Description of the simulations

The algorithm for molecular dynamics simulations has been used elsewhere [24]. The boundaries are configured

so that there is a pair of parallel vibrating walls that are perpendicular to gravity (Z direction) $g = 9.8 \text{ m/s}^2$. The system is periodic in the horizontal directions (XY coordinates). The particles interact through a combination of a conservative restoring force and normal and tangential frictional forces, in such a way that particle-particle forces can be expressed as

$$\begin{aligned} \mathbf{F}_{ij}^{\text{rest}} &= Y m_i (|\mathbf{r}_{ij}| - \sigma) \hat{\mathbf{r}}_{ij}, \mathbf{F}_{ij}^{\text{diss}} = -\gamma_n m_i \mathbf{v}_{ij}^n, \\ \mathbf{F}_{ij}^{\text{shear}} &= -\gamma_s m_i \mathbf{v}_{ij}^t. \end{aligned}$$

In the above equations, subscripts i, j stand for particles; m_i is the particle mass; \mathbf{r}_{ij} are relative positions: $\mathbf{r}_{ij} = \mathbf{r}_i - \mathbf{r}_j$, and $\hat{\mathbf{r}}_{ij} = \mathbf{r}_{ij}/|\mathbf{r}_{ij}|$, with $F_{ij} = 0$ if $r_{ij} = |\mathbf{r}_{ij}| > \sigma$. Analogously, \mathbf{v}_{ij} stands for relative velocities, and $\mathbf{v}_{ij}^n, \mathbf{v}_{ij}^t$ stand for the projections of relative velocities in the normal and tangential directions respectively. The coefficient Y is the Young modulus that characterizes the (conservative) restoring force whereas γ_n, γ_s account for the dissipation in the normal and tangential directions respectively. There is also a set of analogous particle-wall interactions, but with coefficients $Y_w, \gamma_{nw}, \gamma_{sw}$. Analogous equations would rule for the wall-particle interactions, but with coefficients $Y_w, \gamma_{nw}, \gamma_{sw}$ respectively, which can take in the code different values to those for particle-particle interactions. Analogously, particle-wall interactions are null if $r_{iw} > \sigma/2$, where r_{iw} is the distance between the i -th particle and the wall. In this work we have used values of parameters that mimic the behavior of metallic balls with a coefficient of normal restitution $\alpha = 0.95$ for steel balls [29]. Also, in order to simplify, we have used the same values of force parameters for the wall-particle interactions. Thus, use here $Y = Y_w = 10^7 \text{ s}^{-2}$, $\gamma_n = \gamma_{nw} = 200 \text{ s}^{-1}$, $\gamma_s = \gamma_{sw} = 100 \text{ s}^{-1}$. See [37] for further reference. Other simulation parameters are $\nu = 640 \text{ Hz}$, and $h = 1.75 \sigma$. Other simulation parameters are $\nu = 643.22 \text{ Hz}$, and $h = 2.00 \sigma$, where $\sigma = 3/64 \text{ in} \simeq 1.190625 \text{ mm}$, and the 2D number density is $\rho_{2D} = 0.433$.

Molecular dynamics simulations were performed trying to mimic the experimental conditions [24], by adjusting the friction coefficients to the values that approximately would correspond to steel spheres [38].

Appendix C: Implementation of the Kovacs Protocol in Experiments and Simulations

This section describes the procedure used to implement the Kovacs protocol, which is identical in the experiments and simulations. The protocol consists of the following five steps:

1. Determine the two steady states associated with the initial and final input accelerations—the upper and lower steady states shown in Fig. 1. These values correspond to $\Gamma_0 = 7.0$ and $\Gamma_f = 3.15$ respectively in the experiments and to $\Gamma_0 = 12.5$ and $\Gamma_f = 5.0$ respectively in the simulations.
2. Measure the steady states for the intermediate acceleration values used in the experiments, $\Gamma_w = \{6.5, 6.0, 5.5, 5.0, 4.5, 4.0\}$ (and in simulations, $\Gamma_w = \{11.5, 10.5, 9.5, 8.5, 7.5, 6.5, 5.5\}$), and obtain the corresponding steady horizontal temperatures $\{T_s^*(\Gamma_w)\}$ in both experiments and simulations.
3. Record statistical realizations of the relaxation dynamics toward the lower-acceleration steady state ($\Gamma_f = 3.15$ for experiments, $\Gamma_f = 5.0$ in the simulations), starting from the steady state at the upper acceleration ($\Gamma_0 = 7.0$ for the experiments, $\Gamma_0 = 12.5$ in the simulations).
4. Construct relaxation curves by selecting points along the relaxation obtained in step 3 whose final temperatures match $T = \{T_s^*(\Gamma_w)\}$, using the $\Gamma_0 = 7.0$ and $\Gamma_0 = 12.5$ (experiments and simulations respectively) steady state as the initial condition.
5. Generate the Kovacs response curves by initiating the system from the final states identified in step 4, by applying the intermediate accelerations and recording the evolution until the steady values $\{T_s^*(\Gamma_w)\}$ are reached.